An Original Precipitation Route toward the Preparation and the Sintering of Highly Reactive Uranium Cerium Dioxide Powders

J. Martinez [a,b], N. Clavier [a,*], A. Mesbah [a], F. Audubert [b], X.F. Le Goff [a], N. Vigier [c]

and N. Dacheux [a]

[a] ICSM, UMR 5257 CEA/CNRS/UM2/ENSCM, Site de Marcoule Bât. 426, BP 17171, 30207 Bagnols/Cèze cedex, France
[b] CEA, DEN, Cadarache, DEC/SPUA/LTEC, Bât 717, 13108 St Paul lez Durance, France
[c] AREVA NC/BG Aval/DO Recyclage/RDP, Boîte à lettre 3747C-1, 1 Place Jean Millier, 92084 Paris La Défense, France

* Corresponding author :

Dr. Nicolas CLAVIER

ICSM – UMR 5257 CEA/CNRS/UM2/ENSCM

Site de Marcoule – Bât 426

BP 17171

30207 Bagnols sur Cèze

France

Phone : + 33 4 66 33 92 08

Fax : + 33 4 66 79 76 11

nicolas.clavier@icsm.fr

Abstract:

The preparation of dense $U_{1-x}Ce_xO_2$ mixed dioxides pellets was achieved from the initial precipitation of highly reactive precursors. In a first step, a wet chemistry route, based on the mixture of U^{4+} and Ce^{4+} in acidic solution with large excess of NH_4OH, was set up to reach the precipitation of the cations. The solid phase was then dried under vacuum to avoid aggregation phenomena. Further characterization of the powders by XRD, EDS and TEM revealed the formation of hydrated $U_{1-x}Ce_xO_2.nH_2O$ that probably resulted from the ageing of hydroxide compounds. Also, microscopy investigations evidenced the nanosized character of the powder which was associated to high values of specific surface area, typically in the 100-150 $m^2.g^{-1}$ range.

The behavior of $U_{1-x}Ce_xO_2.nH_2O$ versus temperature was investigated in a second part. If the increase of the heat temperature allowed one to observe an improvement of the crystallization state linked with the growth of crystallites, it was also accompanied by a strong decrease of the powders reactivity. On this basis, sintering tests were conducted in reducing atmosphere on the compounds as prepared. Dilatometry experiments indicated a low densification temperature compared to other ways of preparation reported in the literature. Also, the pellets prepared after firing at different temperatures (1350°C-1550°C) showed that a wide range of microstructures was achievable. Particularly, bulk materials with densities of 90-95 % of the calculated value could be prepared with average grain size ranging from around 100 nm to more than 5 μm. This simple process of elaboration of dense materials from highly reactive hydrated oxide precursor thus appears as a very interesting way to prepare actinide oxides materials.

Introduction

Actinides mixed dioxides, such as $(U,Pu)O_2$, are currently employed as fuels in several LWR-type nuclear reactors and are considered as the reference fuel material for several Gen-IV concepts, including Sodium-cooled Fast Reactor (SFR) [1]. In this perspective, homogeneous fuel pellets will be needed to avoid the presence of local aggregates with high plutonium concentration that can decrease the performance of the fuel during its life-cycle [2] and partly hinder its reprocessing due to the strong resistance to dissolution of PuO_2 [3]. As the processes based on powder metallurgy, i.e. mechanical mixture of powders, were generally associated to an heterogeneous distribution of the cations at the micron scale [4], numerous studies were devoted to the exploration of new ways of preparation *via* wet chemistry routes. These methods are frequently based on the initial precipitation of crystallized precursors that ensure the simultaneous incorporation of cations thus their homogeneous distribution within the crystal structure (solid solutions).

Among such precursors, carbonates [5], nitrates [6], and more importantly oxalates [7], were particularly investigated and already provided interesting properties such as a rapid preparation of the powders [8, 9] and a simple conversion to the desired oxide phase through heat treatment at high temperature. However, the final powders obtained were found to present a contrasted behaviour concerning their sintering capability. On the one hand, the initial use of wet chemistry methods was generally correlated to a decrease of the temperature required to obtain dense pellets (i.e. reaching about 95% of the calculated value), which was reported in several cases to drop down from 100 to 200°C compared to the reference processes [9]. On the other hand, in spite of this good sintering capability, several drawbacks also arose from the use of powders coming from the conversion of low-temperature precursors. Among them, for instance, the crystallized compounds obtained during the precipitation step frequently exhibit an oriented morphology (needle- or plate-like grains), which could weaken the mechanical properties of the pellet in the absence of an additional grinding step.

In this context, it was more than surprising to remark that the preparation of hydroxide compounds was poorly reported in the literature for the preparation and the sintering of actinide oxide powders. Indeed, the hydroxylation of actinides is well-known to be the first step leading to the formation of colloids in solution, which further aggregate to yield nanoparticles [10, 11]. The use of hydroxide-based powders could then appear as an interesting alternative in order to get highly reactive and carbon-free oxide powders after conversion of the precursors. Moreover, owing to the nanosize of the starting powders, one can expect to reach a larger range of microstructures involving high values of relative density coupled either with small (typically below 1 µm) or large (over 10 µm) grains. In these conditions, the average grain size and the subsequent grain boundaries distribution could be

tailored to further orientate several properties in use of the nuclear fuel such as thermal conductivity [12], mechanical behaviour [13], or fission gases retention [14].

This paper then reports the preparation of (U,Ce)O$_2$ mixed dioxides from the initial precipitation of hydroxide compounds, cerium being used in a first step as a surrogate of plutonium [15]. Along with the description of the synthesis route, a complete characterization of the precursors and their conversion to dioxides was undertaken by the means of *in situ* techniques, including HT-PXRD. Finally, the behaviour of the as-prepared powdered samples was investigated during sintering under reducing atmosphere through dilatometric measurements and SEM observations.

1. Experimental

Synthesis.

Hydrochloric uranium (IV) solution was prepared by dissolving uranium metal chips (obtained form CETAMA) in concentrated hydrochloric acid. The metal pieces were first washed in 2M HCl to remove possible traces of uranium oxide present at the surface, rinsed with water and ethanol and finally dissolved in 6M HCl. The concentration of the solution was finally estimated to 0.47 ± 0.01 M using the titration method developed by Dacheux *et al.* [16, 17]. Other reagents (NH_4OH and $Ce(SO_4)_2$) were of analytical-grade and used as supplied by Sigma-Aldrich.

The preparation of the initial hydroxide precursors started from a mixture of the hydrochloric uranium (IV) solution (prepared as described above) and of cerium (IV) sulfate (≈ 0.05 M), in the desired stoichiometric ratio x = Ce/(U + Ce). Such mixture was then poured into a large excess of ammonium hydroxide (400%) at room temperature, leading to the instantaneous formation of a precipitate. This latter was further aged in solution for one hour under magnetic stirring.

The powders precipitated were then separated from the supernatant by centrifugation at 4500 rpm. Optimal conditions were chosen from the determination of the size cut-off, assuming that the grains of the different phases were spherical [18] :

$$r = \sqrt{\frac{9s\eta}{2(\rho_2 - \rho_1)}} \qquad (1.)$$

Where :   r is the radius of the particles;

s the coefficient of sedimentation (in $s.m^{-2}$);

η the viscosity of the liquid media (10^{-3} $kg.m.s^{-1}$ for water at room temperature);

ρ_1 the density of the liquid phase (1 $g.cm^{-3}$ for water);

and ρ_2 the density of the particles (equal to 7.65 $g.cm^{-3}$ for CeO_2 and 10.97 $g.cm^{-3}$ for UO_2 [19]).

On this basis, the experimental conditions considered corresponded to a cut-off from about 20 to 30 nm depending on the chemical composition of the samples considered. The

freshly prepared precipitates were finally washed several times with deionized water then once with ethanol in order to eliminate remaining traces of ammonium hydroxide.

After this washing step, the hydroxide precursors underwent a de-agglomeration process aiming to avoid the presence of large aggregates that can strongly decrease the reactivity (thus the sinterability) of the powders. In this purpose, samples were introduced into a flask with 50 mL of ethanol, which is commonly used as a polar protic solvent during de-agglomeration processes [20], and allows a rapid evaporation at low temperature that can prevent any coarsening of the particles. The suspension of powder in ethanol was then placed under vacuum and stirred mechanically at 40°C. After the complete evaporation of the solvent, stirring was maintained for a few minutes, then the flask was filled with nitrogen in order to avoid the oxidation of uranium (IV). For the same reason, the powdered precursor obtained was further stored under inert atmosphere.

For all the chemical compositions investigated, the supernatants collected after the precipitation step were analyzed by Inductively-Coupled Plasma Atomic Emission Spectroscopy (ICP-AES, Spectro Arcos) to determine the precipitation yield of the cations. During measurements, several wavelengths were considered for each element, i.e. $\lambda = 448.691$ nm, 418.660 nm, 413.765 nm and 413.380 nm for cerium and $\lambda = 385.958$ nm, 409.014 nm, 367.007 nm and 279.394 nm for uranium in order to avoid any interference. From the results obtained, the precipitation of both cations appeared systematically to be quantitative, with yield values ≥ 99 %.

Characterization.

Powder X-Ray Diffraction (PXRD) patterns were obtained by the means of a Bruker D8 diffractometer equipped with a Lynx-eye detector adopting the parallel geometry (reflection mode), and using Cu K$\alpha_{1,2}$ radiation ($\lambda = 1.54184$ Å). PXRD patterns were recorded at room temperature in the $5° \leq 2\theta \leq 120°$ range, with a step size of $\Delta(2\theta) = 0.03°$ and a total counting time of about 2.5 hours. For *in situ* high temperature experiments, powders were placed in dedicated alumina boats and heated with a rate of $10°C.min^{-1}$, under He/4% H$_2$ atmosphere. HT-PXRD patterns were recorded each 50°C from 30 to 500°C then with a 100°C step from 500°C to 1000°C. Temperature was held 15 minutes before recording the pattern in order to ensure the thermodynamic equilibration of the sample.

All the PXRD patterns were refined by the Rietveld method using the Cox-Hastings pseudo-Voigt profile function [21] implemented in the Fullprof_suite program [22]. During all the refinement, the conventional profile/structure parameters (zero shift, unit cell parameters, scale factors, global thermal displacement and asymmetric parameters) were allowed to vary. Moreover, for each phase, modelling of the intrinsic microstructure parameters was performed by applying an anisotropic size model.

Scanning Electron Microscope (SEM) observations were directly conducted on powdered samples or on sintered pellets without prior preparation such as metallization, using a FEI Quanta 200 electronic microscope, equipped either with an Everhart-Thornley Detector (ETD) or a Back-Scattered Electron Detector (BSED), in high vacuum conditions with a very low accelerating voltage (2 – 3.1 kV). These conditions were chosen in order to create a beam deceleration effect that led to high resolution images.

The chemical composition of the samples were checked by the means of Energy Dispersive Spectrometry (EDS) coupled with the SEM device using an optimal working distance of 10.7 mm and an acceleration voltage of 15 kV. In order to get a quantitative information, UO_2 and CeO_2 were used as external standards, using the φRhoZ model for correction. Prior to the analyses, each compound was coated with an epoxy resin, polished and finally metallized by carbon deposition. EDS analyses were then undertaken considering fifty data acquisitions randomly performed at the sample surface. For each measurement, a dwell time of 60 seconds was considered, resulting in a counting statistics of about 10000 counts.

In the case of powdered samples, SEM observations were also correlated with specific surface area measurements using adsorption/desorption of N_2 at 77 K (BET method) by the means of a Micromeritics Tristar 3020 apparatus. Prior to the analyses, samples were outgassed at 90°C for 4 hours in order to ensure the release of water molecules adsorbed at the surface of the solids.

TEM observations and EDS analyses were performed with a JEM-2200FS high-resolution TEM operating at 200 kV. Images were acquired with a Gatan Ultrascan 4000 camera. EDS measurements were made with a JEOL SDD 30 mm^2 HyperNine (138 eV). For analysis, 0.5 mg of powder was suspended in ethanol (2 mL), then a drop was deposited onto a carbon copper grid. Crystallographic analyses were made with Fiji software [23] by using Fast Fourier Transform on the high resolution pictures. Particle size distribution was evaluated by measuring more than fifty particles observed on different pictures.

Thermal analyses and sintering.

Thermogravimetric analyses were undertaken thanks to a Setaram Setsys Evolution equipped with a type-W5 thermocouple (W-5%Re / W-26%Re) and dedicated to analyses performed under reducing atmosphere (Ar/2% H_2). After recording a baseline using an empty alumina crucible (25 µL), weight loss was measured during a heat treatment up to 1000°C with a rate of 10°C.min^{-1}. Similarly, dilatometric measurements were conducted on a Setaram Setsys Evolution apparatus. In this case, heat treatments were undertaken under Ar/2% H_2 flux up to 1600°C with a rate of 10°C.min^{-1}. Dwell time of 30 minutes was then considered before sample was cooled down to room temperature at 30°C.min^{-1}. For both thermogravimetric and dilatometric analyses, the gaseous species emitted during the heat treatment were analysed by the means of Hiden Analytical QGA analyser using mass spectrometry.

Finally, density measurements of the sintered pellets were conducted through geometrical measurements using a precision calliper. These values were further used to estimate the global porosity of the samples.

2. Results and discussion

2.1. Characterization of the precursors

The literature concerning the hydrolysis of uranium(IV), and more generally that of tetravalent actinides, is abundant as numerous data concerning the associated thermodynamic constants, particularly solubility products have been reported [11, 24, 25]. However, the precise nature of the solid phases formed remains widely unclear. If the use of high temperatures (typically above 700°C) led to the formation of well-crystallized and anhydrous UO_2 [26], the products prepared at room temperature are either referred as hydroxydes or hydrated oxides [10]. The precipitation can thus be written either as:

$$U^{4+} + 4\ OH^- \leftrightarrow U(OH)_4 \qquad (2.)$$

or

$$U^{4+} + 4\ OH^- \leftrightarrow UO_2 \cdot xH_2O + (2\text{-}x)\ H_2O \qquad (3.)$$
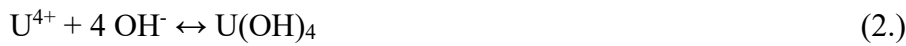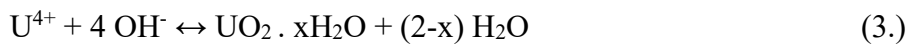
The powdered samples obtained after the synthesis procedure described above and further de-agglomeration step were then first investigated by the means of Powder X-Ray Diffraction (PXRD). For all the chemical compositions considered, the PXRD patterns collected (Figure 1) exhibited wide XRD lines (large FWHM) that fit with the cubic fluorite-type structure (Fm-3m space group), characteristic of both CeO_2 [27] and actinide dioxides [28]. From these data, the precipitation of a partly amorphous hydrated oxide was found to be the most credible hypothesis, albeit the formation of such compound could also occur through the ageing of an initial hydroxide form, for example during the drying procedure, considering the following reaction:

$$U_{1\text{-}x}Ce_x(OH)_4 \rightarrow U_{1\text{-}x}Ce_xO_2 \cdot nH_2O + (2\text{-}n)\ H_2O \qquad (4.)$$
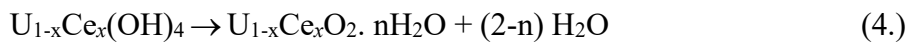
Also, additionnal Raman experiments (not presented here), confirmed the absence of hydroxyl groups in the samples, as well as the precipitation of uranium under its tetrapositive state.
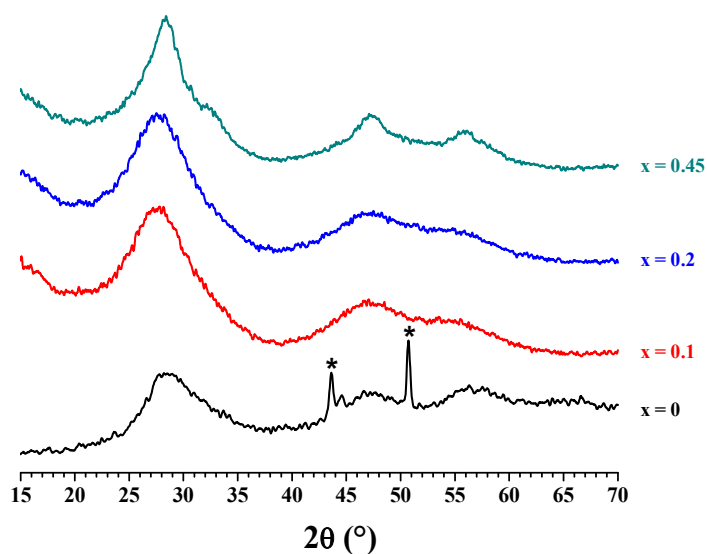
Figure 1. XRD patterns of the $U_{1-x}Ce_xO_2 \cdot n\ H_2O$ (x = 0, 0.1, 0.2, 0.45) precursors. Main diffraction lines of sample holder are indicated by a star (*).

The large width of the peaks recorded revealed that the samples prepared were poorly crystallized and/or nanosized. This feature was confirmed by the Rietveld refinement of the PXRD which allowed the determination of the coherent length domains (i.e. average crystallite size). Only small variations of the average crystallite size were observed depending on the chemical composition considered, with values ranging from 1.0 nm for x = 0 to 1.5 nm for x = 0.45. In these conditions, the incorporation of cerium in the structure could appear to slightly increase the crystal growth during the precipitation process. Such modification could be linked to the presence of small amounts of trivalent cerium in the solid that could increase the diffusion of cations [29, 30].

The morphology of the hydroxide precursors was then investigated by the means of scanning (SEM) and transmission (TEM) electron microscopies. Whatever the chemical composition considered, the SEM micrographs recorded (Figure 2) systematically revealed a similar aspect. The powdered samples were found to be composed of very small particles with a size in the nanometer range. In spite of the drying step performed under vacuum, some large aggregates (ranging from 10 to 20 µm) still remain. They should result from the preparation

10

of the sample before the observation (deposition on a carbon stick) and/or from the high vacuum used in the SEM chamber. Still, despite of the partial aggregation of the nanosized crystallites, specific surface area measurements through the BET method confirmed the very high reactivity of the powders prepared. Indeed, the values obtained all ranged between 130 and 150 $m^2.g^{-1}$, again independently from the cerium incorporation rate considered.

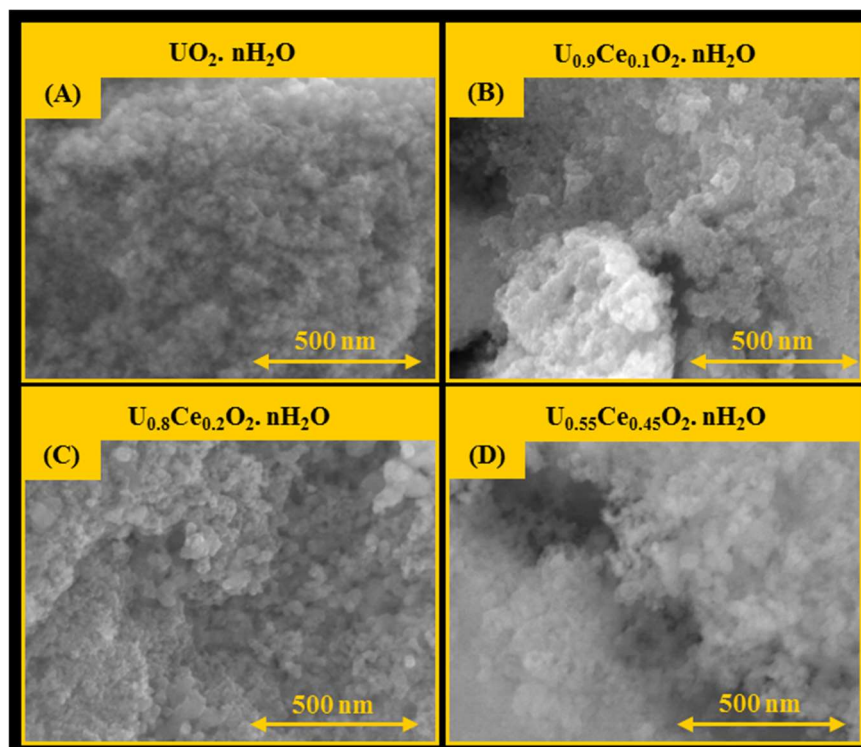**Figure 2.** Scanning electron micrographies of powdered $U_{1-x}Ce_xO_2 . nH_2O$ with x = 0 (A), x = 0.1 (B), x = 0.2 (C) and x = 0.45 (D).

In order to complete the SEM observations of the hydroxide powders, and particularly to investigate more precisely the crystallization state and the chemical composition of the crystallites observed, TEM micrographs were also performed (Figure 3). First of all, the images recorded in the bright field mode confirmed the nanosized character of the powders studied. Indeed, the size of the crystallites observed on the micrographs generally reached between 2 and 5 nm (Figure 4) which fits with the results obtained through XRD Rietveld refinement, owing to the uncertainties of both techniques.

Additionally, nanodiffraction patterns were also collected from one of the samples studied (x = 0.1) and confirmed the polycrystalline nature of the sample (Figure 3B). Indeed, the interactions of the primary electrons with several crystallites presenting different orientations led to the formation of diffraction cones that led to the apparition of circles on the

final diffraction pattern. The comparison of the ratio of the circles' diameter (Dn/D1) (Table S1) with several compounds of reference [31] led to assign the crystal structure to a face centered cubic system. This result then appeared in good agreement with the ageing of the initial hydroxide precipitates into hydrated dioxides, which adopt the classical fluorite-type structure of CeO_2 and AnO_2 compounds.
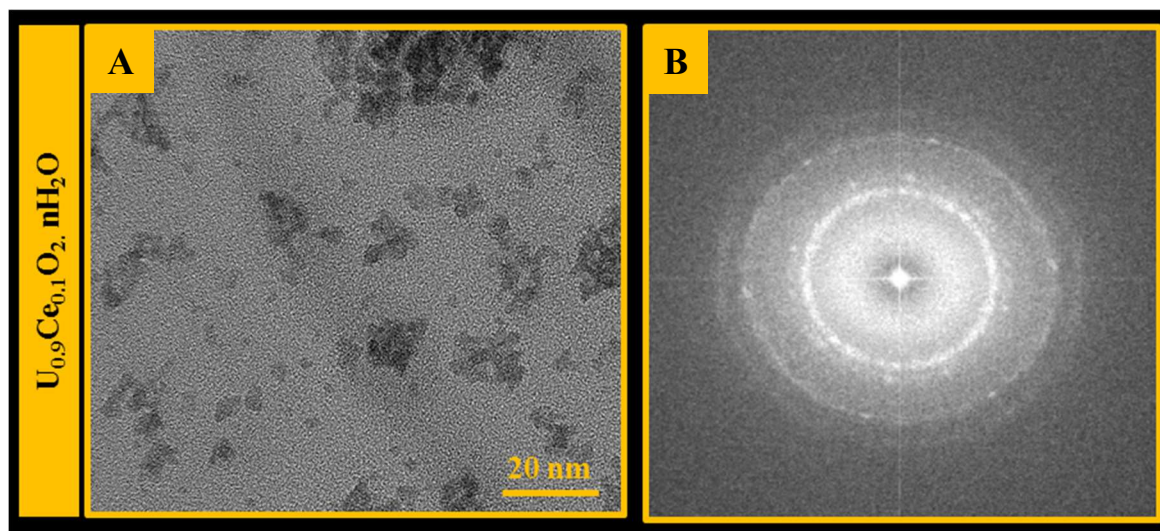

Figure 3. TEM micrographs (A) and diffraction circles (B) of powdered $U_{0.9}Ce_{0.1}O_2.$ nH_2O.
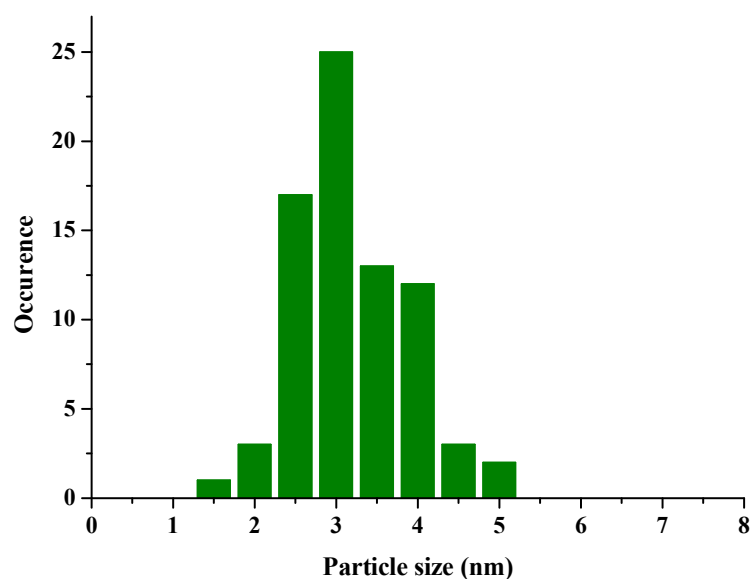
Figure 4. Statistical variations (N = 75) of the particles size in $U_{0.9}Ce_{0.1}O_2. nH_2O$.

Finally, EDS analyses were also coupled to both SEM and TEM observations. On the one hand, SEM-EDS measurements allowed the evaluation of the cationic homogeneity of the

powdered samples at the micrometer scale. For all the samples studied, 50 measurements were then randomly performed at the surface on the sample and were considered to be representative of the statistical distribution of the Ce/(U + Ce) mole ratio, corresponding to the cerium distribution within the sample. Whatever the chemical composition considered, the data obtained were fitted with a single Gaussian law (Figure S1). This mathematical treatment first led to determine the average chemical composition of the samples which was found to be in a very good agreement with that calculated (Table 1). The precipitation of the hydroxide precursors can thus be considered to be quantitative. Also, the distribution of the analyses results around the average value appeared to be limited, thus evidencing the very good homogeneity of the samples prepared at the micrometer scale. As a matter of comparison, the distribution of the Ce/(U+Ce) mole ratio was found to be significantly narrowed compared to the results reported for $(Th,U)O_2$ mixed oxides prepared from oxalate precursors, even when using hydrothermal conditions [9].

Table 1. Results of statistical EDS analyses obtained for $U_{1-x}Ce_xO_2 . nH_2O$ samples.

$x_{calc.}$	U (wt.%)	U (at.%)	Ce (wt.%)	Ce (at. %)	$x_{exp.}$
0.1	72.0 ± 0.3	30.0 ± 0.1	5.0 ± 0.3	3.3 ± 0.2	0.10 ± 0.01
0.2	63.9 ± 0.3	26.7 ± 0.1	9.7 ± 0.3	6.7 ± 0.2	0.20 ± 0.01
0.45	44.5 ± 0.3	18.3 ± 0.1	21.1 ± 0.3	15.0 ± 0.2	0.45 ± 0.01

Evidence for this homogeneity was further strengthened through the EDS measurements coupled with TEM experiments. Thanks to this set up, qualitative analyses were conducted on several single dispersed crystallites and systematically revealed the simultaneous presence of uranium and cerium. These results confirmed that the hydroxide precipitation of the cations within our operating conditions did ensure the formation of mixed precursors and was not affected by some hypothetic differences in the kinetics of precipitation of Ce^{4+} and U^{4+}. Also, it confirmed that the good homogeneity pointed out by EDS measurements truly came from the formation of a $U_{1-x}Ce_xO_2 . nH_2O$ solid solution at the nanometer scale and did not result from an artefact coming from the high number of particles embedded in the volume analyzed.

2.2. Conversion of the hydroxide precursors

The second part of the study was devoted to the thermal conversion of the precursors into high temperature $(U,Ce)O_2$ samples. In this aim, TG analyses were first performed under

reducing atmosphere (Ar+5%H_2) to evidence the reaction scheme driving the conversion of precursors into final dioxides. As an example, the thermogram recorded for $U_{0.9}Ce_{0.1}O_2$. nH_2O presented on figure 5 while data obtained for other compositions are supplied as supplementary data (see figure S2). Whatever the amount of cerium in the sample, the weight loss curve exhibited two distinct steps when heating from room temperature to 500°C. Such behaviour appeared to be characteristic of the transformation of actinides hydroxides / amorphous oxides as it was already pointed out by Yildiz *et al.* during the heat treatment of $(Th,Ce)(OH)_4$ [32]. Nevertheless, the authors did not propose any mechanism explaining such behaviour. In this aim, our experimental setup was also implemented with a mass spectrometer in order to analyse the gases emitted during this thermal treatment. From this data, the first part of the weight loss, detected between room temperature and 280°C, was correlated to the H_2O emission. This first step was then assigned to the full dehydration of the sample and corresponded to the loss of 1.5 H_2O per mole of oxide, resulting in a general formulae of $U_{0.9}Ce_{0.1}O_2$. $1.5H_2O$. This formulation is in good agreement with what was observed in other hydrated uranium dioxide which were obtained from the ageing of hydroxide colloids in solution [33].
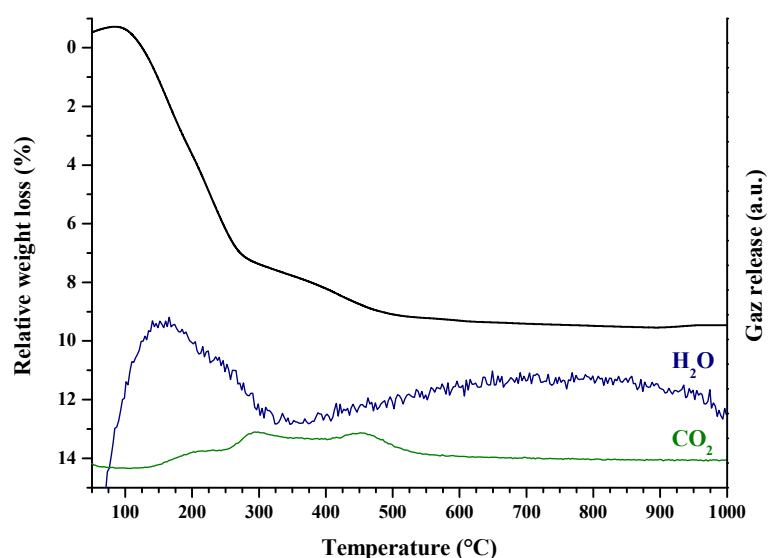

Figure 5.   TG analyses (black) of $U_{0.9}Ce_{0.1}O_2$. nH_2O coupled with the detection of CO_2 (green) and H_2O (blue) by mass spectrometry.

The second step of the thermal conversion of the precursor was further characterized by the detection of CO_2 by mass spectrometry. Such carbon species could evidence the presence of atmospheric CO_2 initially adsorbed onto the surface of the powder, in good agreement with the very high specific area previously mentioned. As already discussed, such high surface reactivity is likely to induce the partial oxidation of uranium (IV). On this basis, and owing to the presence of carbon traces inside the furnace, the CO_2 emission could also result from the reduction of the oxidized U(V) or U(VI) species under Ar/H_2 atmosphere. However, such phenomenon appeared to be almost independent on the uranium content in the sample. This second weight loss (around 9 %) was completed after heating at around 500°C which thus corresponds to the temperature of formation of pure $U_{0.9}Ce_{0.1}O_2$ dioxide.

In parallel of thermogravimetric analyses, the conversion of the hydrated precursor into uranium(IV)-cerium(IV) dioxide was also monitored through HT-PXRD measurements performed under reducing atmosphere ($He+4\%H_2$) (Figure 6A). As the precursor prepared already presented the characteristic XRD lines of the fluorite structure right after precipitation and drying steps, such features were conserved during the whole heat treatment. The increase in temperature only led to a narrowing of the XRD lines, which was associated to the improvement of the sample's crystallinity and to the growth of the crystallites.

Nevertheless, Rietveld refinement of the HT-PXRD data revealed that all the samples prepared presented slight variation in terms of chemical composition which was associated to different crystallite sizes. Up to 800°C, the XRD lines recorded could be only fitted with two contributions (Figure 6B). From this data, the uranium-enriched phase corresponded to the smallest average length of coherent domains size while the biggest crystallites were more likely assigned to cerium-enriched zones. It is still important to note that the shifts observed in the location of the XRD lines only correspond to weak variations (typically of less than 10% on the x value) that occur at a very small scale of the samples. In these conditions, it did not contradict the very homogeneous distribution of the cations at the micrometer scale already evidenced from EDS measurements.

Also, the increase in the average crystallite size was further quantified by Rietveld refinement and presented a two-step variation versus temperature. As previously evidenced in several other oxide-based materials, including $(Th,Ce)O_2$ and $(Th,U)O_2$ [34, 35], the first step (up to 600-700°C) corresponded to the elimination of crystals defects, leading only to a slight variation of the crystallite size from 1 to 10 nm. The second step observed at higher temperatures was assigned to crystallite growth mechanisms, and was associated to a strong variation of the crystallite size, up to 230 nm at 1000°C.
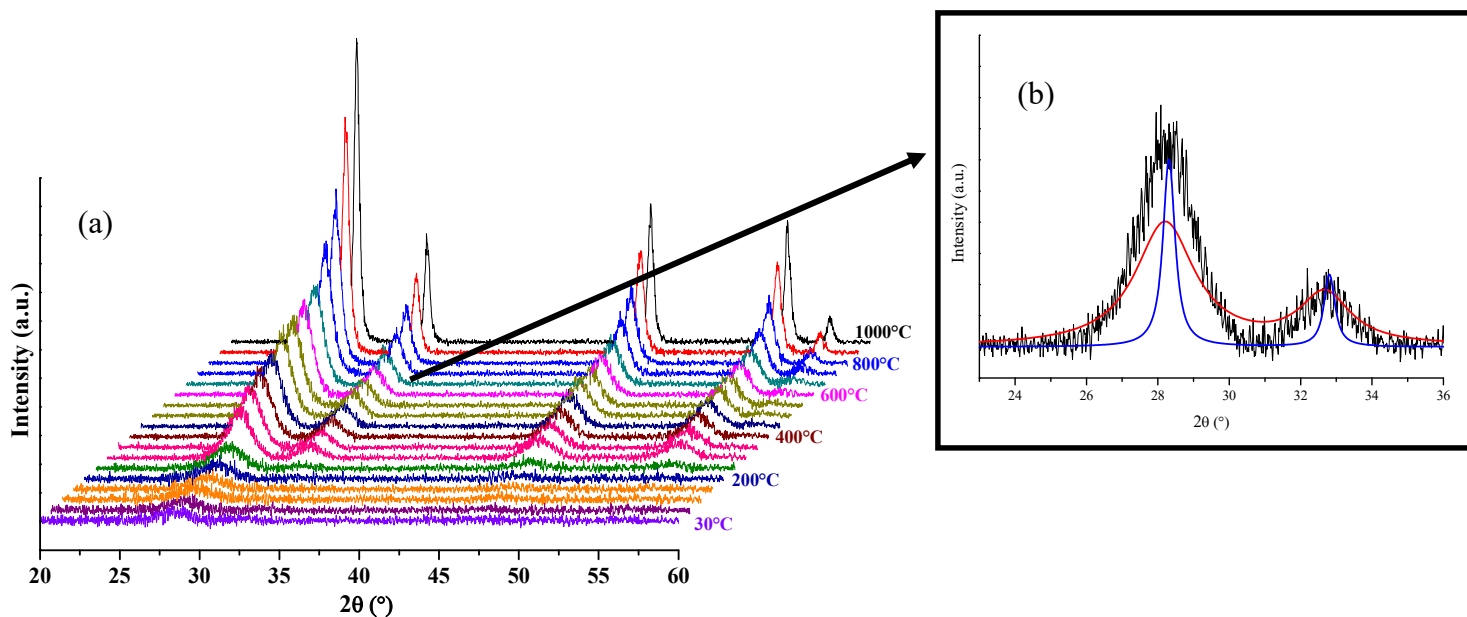
Figure 6. Variation of the XRD diagram of $U_{0.9}Ce_{0.1}O_2 \cdot nH_2O$ versus the heat temperature (a). Example of Rietveld refinement obtained for the pattern recorded at 600°C (b).

In parallel to the HT-PXRD characterization, specific surface area measurements were also performed versus the temperature of conversion (Figure 7) in order to evaluate the decrease in the powder's reactivity generally associated to preliminary heat treatments [9]. For all the samples studied, the S_{SA} value strongly dropped down to about 40 $m^2.g^{-1}$ after firing the powder at 200°C. This important decrease was correlated to the dehydration observed in TG analyses and could result in an agglomeration of the nanosized grains formed during the synthesis. Once the dehydration of the sample completed, i.e. for temperature above 200°C, the specific surface area was found to decrease more gently to finally reach values ranging from 10 to 20 $m^2.g^{-1}$ after heating at 800°C. This second step was thus more likely associated to the increase of the average crystallite size observed by HT-XRD that could also induce some grain growth processes. Indeed, at such temperatures, the nanometric particles observed initially could assemble both through mechanical rearrangements or diffusion processes to results in larger grains [36].
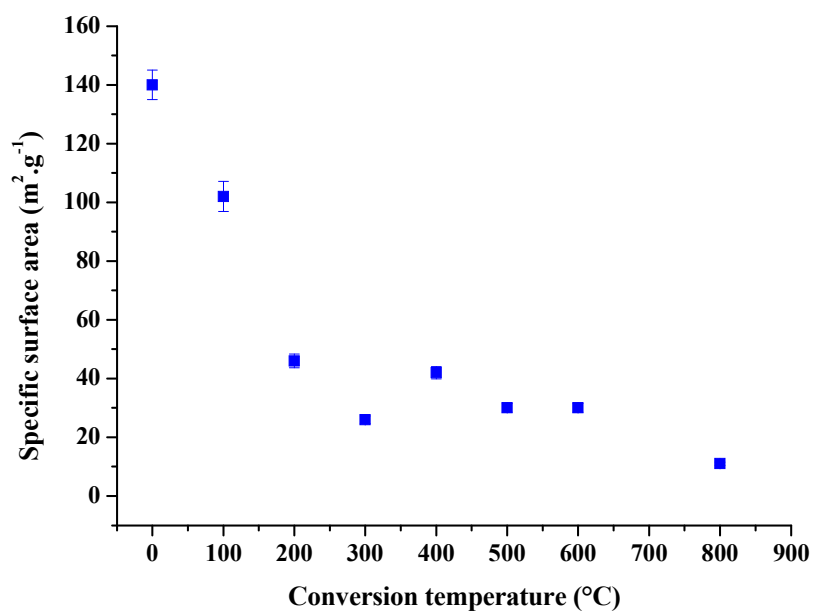
Figure 7. Variation of the specific surface area of $U_{0.9}Ce_{0.1}O_2 \cdot nH_2O$ versus the heating temperature during its conversion into anhydrous and crystalline dioxide (Ar/H_2 2%).

3. Sintering of uranium-cerium hydrated oxides

Owing to the very high specific surface area of the precursors prepared and to the loss of reactivity observed when heating the raw powders, green pellets were directly shaped from raw precursor powders, i.e. hydrated oxides. Hence, $U_{1-x}Ce_xO_2 \cdot nH_2O$ cylinders of 5 mm diameter and about 1 to 2 mm heigth were prepared by uniaxial pressing (500 MPa) in a tungsten carbide die, leading to green densities generally ranging from 45 to 50% (based on the density values reported for anhydrous oxides). This process thus allows the elimination of several preliminary steps frequently used in the fabrication of ceramic materials, such as grinding or pre-heating.

The sintering of uranium-cerium hydrated oxides was further investigated through dilatometric studies under reducing atmosphere ($Ar/2\% H_2$) in order to precise the temperature corresponding to the complete densification of the samples. It is important to note that under such operating conditions, previous works already demonstrated that cerium was mostly maintained in the tetrapositive state, and that no additional Ce_2O_3 phase was formed [37]. Figure 8 presents the relative linear shrinkage measured during the heat treatment of various $U_{1-x}Ce_xO_2 \cdot nH_2O$ samples up to 1600°C, as well as the associated variation of their relative density. For the latter, only the 800-1600°C range was presented as the density of the initial hydrated oxide remains unknown. Owing to this bias, a significant uncertainty was attached to the calculated density which could explained that values slightly exceeding 100% were obtained.

Whatever the cerium content considered, the general trend of the dilatometric curve always presented two distinct shrinkage steps, occurring between 100 and 400°C, then from 800 to 1400°C, both accounting for about 25% of height decrease. On the one hand, the first shrinkage step was assigned to the dehydration of the samples based on the results obtained from TGA studies. Considering the density of the green bodies, one can assume that such dehydration could occur through open porosity without generating any additional defects, such as cracks and pores, in the pellet. On the contrary, dehydration could enhance the aggregation then the packing of the powder, leading to the densification of the agglomerates through electrostatic processes [38].

On the other hand, the second shrinkage step was assigned to the sintering of the dioxides samples. For this latter, the maximum of the shrinkage rate was reached between

1000 and 1200°C. This range of temperature appeared far lower than that usually reported for the sintering of UO_2 under reducing atmosphere, that generally exceeds 1400°C [39]. The very high reactivity of the powders prepared appeared to decrease significantly the temperature of sintering of the final ceramic materials in the operating conditions chosen.
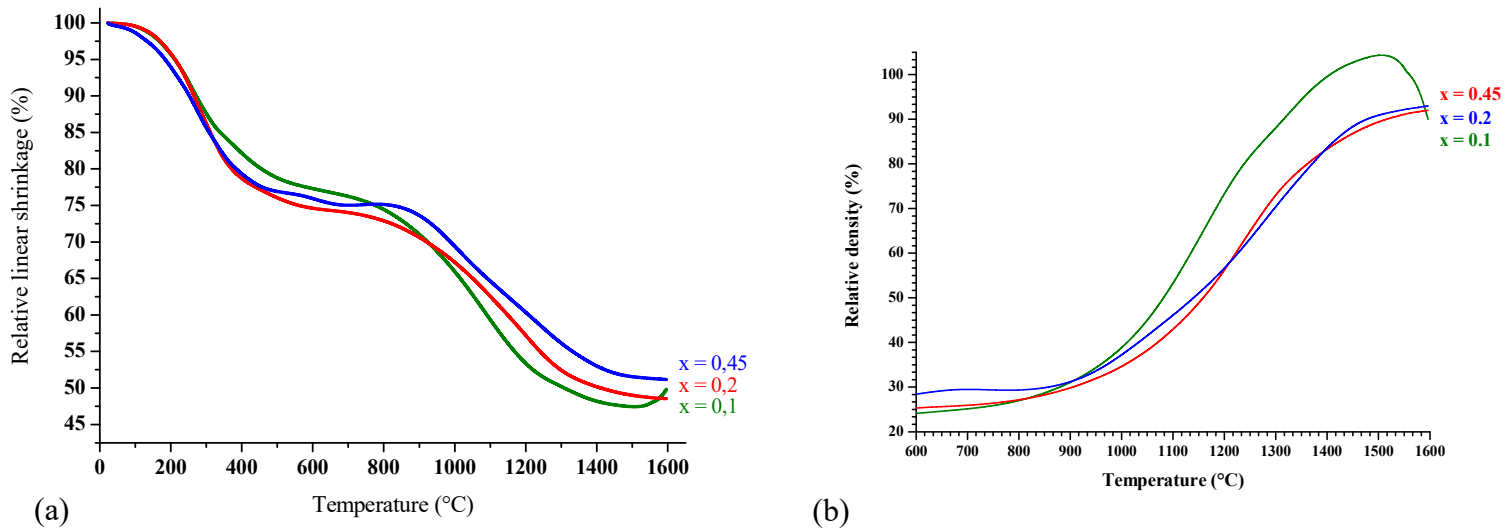

Figure 8. Dilatometric study (a) and variation of the relative density (b) obtained for $U_{1-x}Ce_xO_2$. nH_2O samples : x = 0.1 (green), x = 0.2 (red), x = 0.45 (blue).

Finally, the microstructure of the $U_{1-x}Ce_xO_2$ oxide pellets was investigated by the means of SEM observations and geometrical measurements. For that purpose, sintering was achieved through heating treatments at various temperatures (1350, 1450 and 1550°C) during 8 hours under Ar/H_2 atmosphere. In these conditions, the values determined for the density of the compact bodies are gathered *versus* the sintering temperature in Table 2. As it should have been expected, an increase in the geometrical density was observed concurrently to that of temperature, whatever the chemical composition of the samples. However, the densification appeared to mainly take place between 1350 and 1450°C, where the density increased from about 80% of the calculated value to 90%. Densification was then found to be more moderate between 1450 and 1550°C, leading to final values of geometrical densities closed to 95%.

This value, close to that usually required for nuclear fuels operating in PWR reactors, demonstrates that the initial preparation of hydrated $U_{1-x}Ce_xO_2$. nH_2O precursors could be considered as an interesting alternative that allows the elimination of several intermediate steps. Also, the temperature required to reach high values of relative density appeared to be significantly lower than that usually reported in comparable atmosphere, which are more likely in the 1600-1700°C range [39].

Table 2. Variation of the final relative density of sintered $U_{1-x}Ce_xO_2 \cdot nH_2O$ (with x = 0.1 ; 0.2 and 0.45) pellets for several sintering temperatures.

	Sintering temperature (°C) – 8h		
x	1350	1450	1550
0.1	84.0 ± 1.5	92.0 ± 1.5	94.0 ± 1.5
0.2	78.0 ± 1.5	88.0 ± 1.5	92.0 ± 1.5
0.45	80.0 ± 1.5	91.0 ± 1.5	95.0 ± 1.5

Moreover, SEM observations performed at the surface of the pellets (Figure 9) confirmed the conclusions drawn from the density measurements. On the one hand, the samples sintered at 1350°C exhibit an important amount of open porosity associated to a small average grain size, reaching few hundreds of nanometers. On the other, the compounds sintered at 1450°C no longer presented visible pores at the surface. The important increase in the relative density of the samples measured between 1350 and 1450°C could then be assigned to the elimination of the open porosity, which thus corresponds to the intermediate step of sintering. This decrease of the porosity is also accompanied by a moderate grain growth, leading to an average grain size closed to 1 µm. Grain growth phenomena were further emphasized at 1550°C, where the final average grain size reached up to 5 µm. Also, as no pores were observed at the surface of the pellet, one can assume that the increase in the density observed from geometrical measurements mainly resulted from the partial elimination of the closed porosity.

The development of the pellets microstructure was thus found to follow a classical trend already evidenced for other actinide dioxides, such as ThO_2 [40], with a first step driven by densification and a second one dominated by grain growth. More importantly, the initial precipitation of precursor nanometric particles as precursor allows the preparation of dense pellets (typically in the 90-95 % range) presenting a wide range of average grain sizes, which can be useful to guide several physico-chemical properties of interest of the final ceramic material.
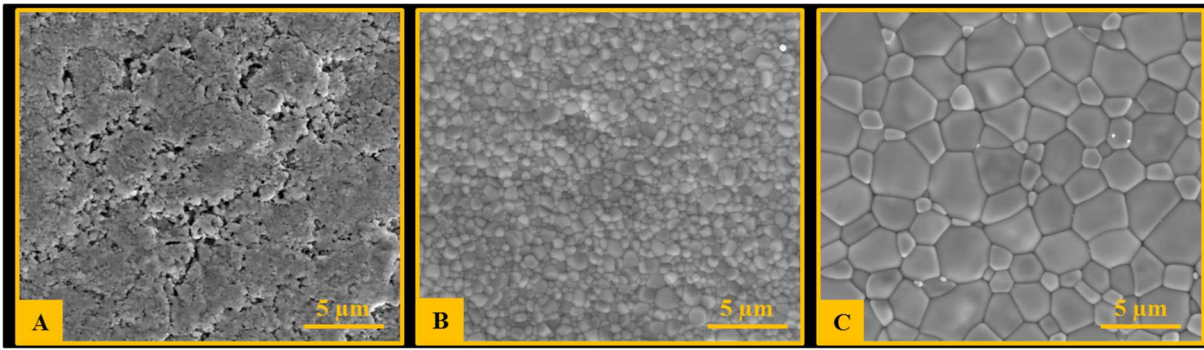
Figure 9. SEM micrographs of sintered pellets of $U_{0.9}Ce_{0.1}O_2 \cdot nH_2O$ obtained after sintering at 1350°C (A), 1450°C (B) and 1550°C (C).

Conclusion

The preparation of highly reactive $(U,Ce)O_2$ precursors was achieved through an easy wet-chemistry route involving hydroxide precipitation followed by a drying step under vacuum. The various characterizations performed on the raw samples prepared revealed the formation of nanosized hydrated oxides, $U_{1-x}Ce_xO_2 \cdot nH_2O$, whatever the cerium incorporation rate considered. Moreover, the precipitation appeared to be quantitative and led to a very homogenous distribution of the cations at the micrometer scale.

The behavior of the $U_{1-x}Ce_xO_2 \cdot nH_2O$ powders *versus* temperature was further investigated and revealed two steps assigned to the complete dehydration of the samples then to the oxides crystallization. Nevertheless, both processes were accompanied by a severe decrease of the specific surface area, due to aggregation and grain growth phenomena. Sintering experiments were then conducted from raw powders, which were found to be the most reactive. This choice also led to avoid potential additional steps such as mechanical grinding or preliminary heat treatments.

The very high sintering capability of the samples prepared was then finally confirmed during densification tests. First, dilatometry experiments pointed out the low temperature required for the efficient sintering of such powders, which was found to be at least 200°C lower than that usually reported in the literature for similar conditions, i.e. strictly reducing atmosphere. The initial precipitation of nanosized powders was also found to lead to versatile microstructure : particularly, bulk materials with densities of 90-95 % of the calculated value could be prepared with average grain size ranging from around 100 nm to more than 5 µm.

This simple process of elaboration of dense materials from highly reactive amorphous hydrated oxide precursor thus appears as a very interesting alternative for the elaboration of actinide oxide ceramic materials. Also, it is now under investigation for other actinides- and lanthanides-based materials as the elaboration of very dense materials with small-grains microstructure should be of significant interest in several other fields, such as for the solid oxide electrolytes used in fuel cells.

Acknowledgements

Supplementary material

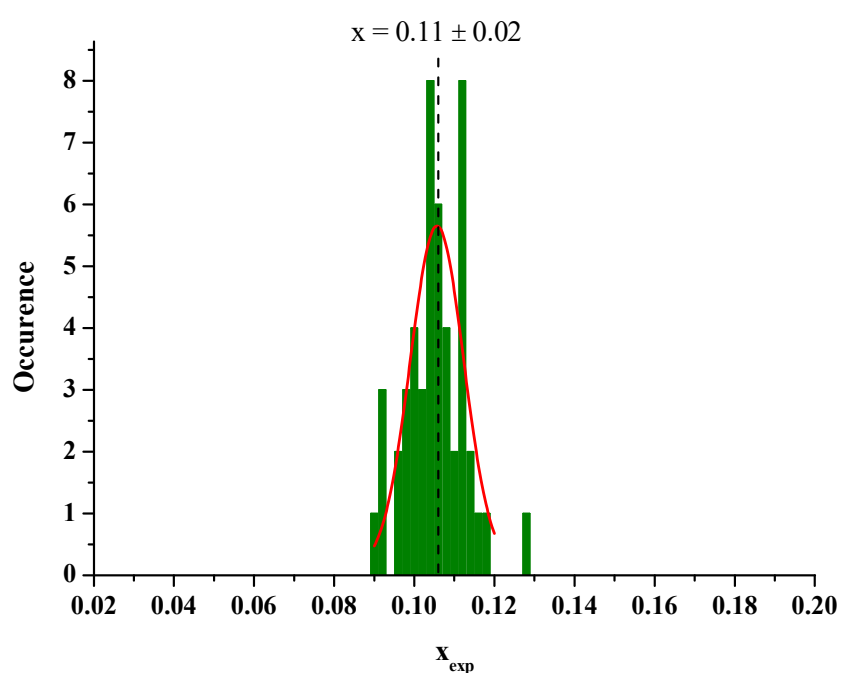**Figure S1.** Statistical distribution of the Ce/(U + Ce) mole ratio (x = 0.1) obtained by EDS analyses with a gaussian representation.
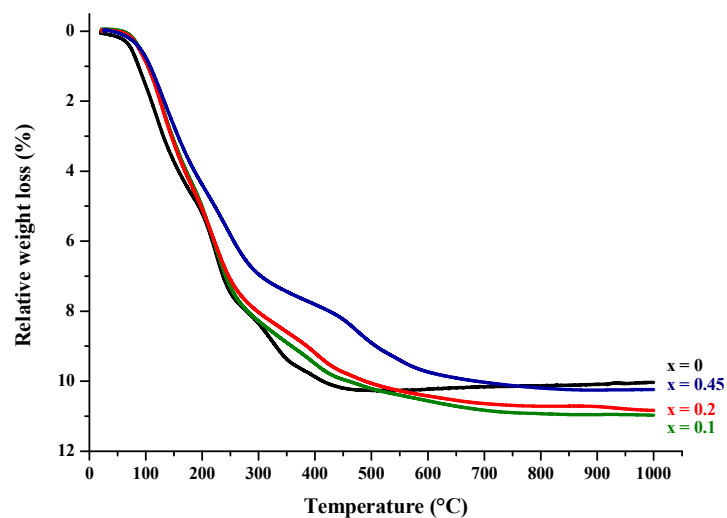
Figure S2. Thermogravimetric analyses of $U_{1-x}Ce_xO_2 \cdot nH_2O$ samples with $x = 0$ (black), $x = 0.1$ (green), $x = 0.2$ (red) and $x = 0.45$ (dark blue).

Table S1. Comparison of the diffraction circles diameter ratio determined from TEM measurements with reference data for UO_2 [31].

	UO_2 (cubic, Fm-3m)	Exp. (SAED)
D2/D1	1.15	1.17
D3/D1	1.63	1.61
D4/D1	1.92	1.93

References

[1] J.E. Kelly, Progress in Nuclear Energy, (2014).

[2] D. Staicu, M. Barker, J Nucl Mater, 442 (2013) 46-52.

[3] G.P. Nikitina, Y.E. Ivanov, A.A. Listopadov, L.B. Shpunt, Radiochemistry+, 39 (1997) 12-25.

[4] G. Oudinet, I. Munoz-Viallard, L. Aufore, M.J. Gotta, J.M. Becker, G. Chlarelli, R. Castelli, J Nucl Mater, 375 (2008) 86-94.

[5] S.K. Kantan, R.V. Raghavan, G.S. Tendolkar, United Nations International Conferences on Peaceful Uses of Atomic Energy, 1958, pp. 132.

[6] B.J.F. Palmer, L.E. Bahen, A. Celli, Am Ceram Soc Bull, 63 (1984) 1030-1034.

[7] F. Abraham, B. Arab-Chapelet, M. Rivenet, C. Tamain, S. Grandjean, Coord. Chem. Rev., 266-267 (2014) 28-68.

[8] N. Hingant, N. Clavier, N. Dacheux, N. Barre, S. Hubert, S. Obbade, F. Taborda, F. Abraham, J Nucl Mater, 385 (2009) 400-406.

[9] N. Hingant, N. Clavier, N. Dacheux, S. Hubert, N. Barre, R. Podor, L. Aranda, Powder Technol, 208 (2011) 454-460.

[10] V. Neck, J.I. Kim, Radiochim Acta, 89 (2001) 1-16.

[11] D. Rai, A.R. Felmy, J.L. Ryan, Inorg Chem, 29 (1990) 260-264.

[12] C. Bagger, M. Mogensen, C.T. Walker, J Nucl Mater, 211 (1994) 11-29.

[13] R.F. Canon, J.T.A. Roberts, R.J. Beals, J Am Ceram Soc, 54 (1971) 105-&.

[14] J.A. Turnbull, C.A. Friskney, J Nucl Mater, 58 (1975) 31-38.

[15] H.S. Kim, C.Y. Joung, B.H. Lee, J.Y. Oh, Y.H. Koo, P. Heimgartner, J Nucl Mater, 378 (2008) 98-104.

[16] N. Dacheux, V. Brandel, M. Genet, New J Chem, 19 (1995) 1029-1036.

[17] N. Dacheux, V. Brandel, M. Genet, New J Chem, 19 (1995) 15-25.

[18] N. Dacheux, J.F. LeDu, V. Brandel, M. Genet, P. Decambox, C. Moulin, New J Chem, 20 (1996) 507-514.

[19] M.T. Hutchings, J Chem Soc Farad T 2, 83 (1987) 1083-1103.

[20] K. Ananthasivan, S. Anthonysamy, A. Singh, P.R. Vasudeva Rao, J Nucl Mater, 306 (2002) 1-9.

[21] P. Thompson, D.E. Cox, J.B. Hastings, Journal of Applied Crystallography, 20 (1987) 79-83.

[22] C. Frontera, J. Rodriguez-Carvajal, Physica B: Condensed Matter, 335 (2003) 219-222.

[23] W. Rasband.

[24] K. Fujiwara, H. Yamana, T. Fujii, H. Moriyama, Radiochim Acta, 91 (2003) 345-350.

[25] C. Manfredi, V. Caruso, E. Vasca, S. Vero, E. Ventimiglia, G. Palladino, D. Ferri, J Solution Chem, 35 (2006) 927-937.

[26] H.D. Greiling, K.H. Lieser, Radiochim Acta, 35 (1984) 79-89.

[27] D. Horlait, L. Claparède, N. Clavier, S. Szenknect, N. Dacheux, J. Ravaux, R. Podor, Inorg Chem, 50 (2011) 7150-7161.

[28] S. Hubert, J. Purans, G. Heisbourg, P. Moisy, N. Dacheux, Inorg Chem, 45 (2006) 3887-3894.

[29] P.-L. Chen, I.W. Chen, J Am Ceram Soc, 79 (1996) 1793-1800.

[30] A. Gotte, D. Spångberg, K. Hermansson, M. Baudin, Solid State Ionics, 178 (2007) 1421-1427.

[31] K. Clausen, W. Hayes, J.E. Macdonald, P. Schnabel, M.T. Hutchings, J.K. Kjems, High Temp. - High Press., 15 (1983) 383-390.

[32] O. Yildiz, J Nucl Mater, 366 (2007) 266-271.

[33] G.I. Nkou Bouala, N. Clavier, R. Podor, J. Cambedouzou, A. Mesbah, H.P. Brau, J. Léchelle, N. Dacheux, Crystengcomm, 16 (2014) 6944-6954.

[34] L. Claparede, N. Clavier, N. Dacheux, A. Mesbah, J. Martinez, S. Szenknect, P. Moisy, Inorg Chem, 50 (2011) 11702-11714.

[35] L. Claparede, N. Clavier, N. Dacheux, P. Moisy, R. Podor, J. Ravaux, Inorg Chem, 50 (2011) 9059-9072.

[36] P. Scardi, M. Leoni, M. Muller, R. Di Maggio, Mat Sci Eng a-Struct, 528 (2010) 77-82.

[37] D. Horlait, A. Feledziak, F. Lebreton, N. Clavier, D. Prieur, N. Dacheux, T. Delahaye, J Nucl Mater, 441 (2013) 40-46.

[38] V. Grechkda, Soviet Powder Metall. Metal Ceram., 15 (1976) 830-832.

[39] T.R.G. Kutty, P.V. Hegde, K.B. Khan, U. Basak, S.N. Pillai, A.K. Sengupta, G.C. Jain, S. Majumdar, H.S. Kamath, D.S.C. Purushotham, J Nucl Mater, 305 (2002) 159-168.
[40] N. Clavier, R. Podor, L. Deliere, J. Ravaux, N. Dacheux, Mater Chem Phys, 137 (2013) 742-749.